

Effects of Charge Exchange in Direct Reactions*

RORY COKER AND TARO TAMURA

The University of Texas, Austin, Texas 78712

(Received 13 February 1969)

The inclusion of charge-exchange effects in direct-reaction theory is discussed and a number of experimental results are then treated: the threshold effect in $^{90}\text{Zr}(d, p)$ and $^{92}\text{Mo}(d, p)$ excitation curves in the region of the (d, n) threshold to the analog of the parent state, and the behavior of the $^{90}\text{Zr}(d, n\bar{p})$ and $^{92}\text{Mo}(d, n\bar{p})$ total cross sections in the same region; Hamburger's data for $^{207}\text{Pb}(d, p)^{208}\text{Pb}$; and, finally, the discrepancy between (d, n) and $(^3\text{He}, d)$ spectroscopic factors for analog states in several light nuclei. The theory is successful in describing the threshold effect and Hamburger's data, but does not explain the discrepancy in spectroscopic factors. A number of methods of calculating the analog-residual-state wave functions are critically discussed.

I. INTRODUCTION

THERE now exists a considerable body of experimental evidence¹⁻¹¹ indicating that the (d, p) reaction channel leading to a given residual nuclear state is coupled to the (d, n) reaction channel leading to the isobaric analog of the residual state excited in (d, p) . The simplest theory of such reactions, originally sketched by Zaidi and von Brentano,¹² and quantitatively extended by Tamura and Watson,¹³ requires replacement of the outgoing nucleon-nucleus state in the usual distorted-wave Born-approximation (DWBA) amplitude by the appropriate linear combination of solutions to coupled Lane equations.¹⁴ The correctness of such an approach can now be given a fairly rigorous test, since a variety of experimental results is available.

In Sec. II, we discuss the introduction of charge-exchange effects into the usual DWBA theory. In Sec. III we discuss the general features of the (d, n) threshold effect observed in (d, p) excitation curves,¹⁻¹¹ the complementary $(d, n\bar{p})$ data of Cue and Richard,¹⁵ and the results of calculations using the theory of

Sec. II. In Sec. IV, the theory is applied to the $^{207}\text{Pb}(d, p)^{208}\text{Pb}$ data of Hamburger,¹⁶ and finally, in Sec. V, the discrepancy in spectroscopic factors obtained with $(^3\text{He}, d)$ and (d, n) reactions to isobaric analog states¹⁷ is studied with three examples, the $^{58}\text{Ni}(d, n)^{59}\text{Cu}$ data of Marusak and Perey,¹⁸ the $^{25}\text{Mg}(d, n)^{26}\text{Al}$ data of Fuchs *et al.*,¹⁹ and the $^9\text{Be}(d, n)^{10}\text{B}$ data of Fuchs and Santo.²⁰ In Sec. VI, we draw some general conclusions concerning the importance of charge exchange in direct reactions, and discuss some problems in the present theoretical description of such reactions.

II. CCBA AMPLITUDE

The scheme for including effects of charge exchange in direct reactions is simply to include the Lane potential¹⁴ $U(r)\mathbf{t}\cdot\mathbf{T}$ in entrance and/or exit channels. Here \mathbf{t} is the isospin of the lighter nucleus, or nucleon, \mathbf{T} is the isospin of the heavier nucleus. There is no effect in a channel where the projectile has $\mathbf{t}=0$, as is the case for deuterons and α particles, but channels with $\mathbf{t}, \mathbf{T}\neq 0$ are coupled, through the Lane equations, with their analogous channels. Thus in (d, n) and (d, p) reactions the $p+N$ and $n+T_-(N)$ final states are coupled. In $(^3\text{He}, d)$ and (t, d) reactions, the $^3\text{He}+N$ and $t+T_-(N)$ initial states are coupled. In reactions such as $(^3\text{He}, p)$ and (t, n) both entrance and exit channels are coupled to their analogous channels.

In what follows, we will consider mainly the (d, n) and (d, p) reactions. The customary DWBA amplitude is given, for (d, p) , by

$$M^{\text{DW}} = \langle \chi_p^{(-)} \phi_n^\alpha | V_{np} | \chi_d^{(+)} \phi_d \rangle. \quad (1)$$

Here $\chi_p^{(-)}$ and $\chi_d^{(+)}$ are the usual distorted waves describing the motion of proton and deuteron, respectively, in the nuclear potential. ϕ_n^α is usually a simple shell-model state, with quantum numbers $\alpha = \{njl\}$, of the stripped neutron, and ϕ_d is the internal

* Research supported in part by the U.S. Atomic Energy Commission.

¹ C. F. Moore, C. E. Watson, S. A. A. Zaidi, J. J. Kent, and J. G. Kulleck, *Phys. Rev. Letters* **17**, 926 (1966).

² W. R. Coker and C. F. Moore, *Phys. Letters* **25**, 271 (1967).

³ R. Heffner, C. Ling, N. Cue, and P. Richard, *Phys. Letters* **26**, 150 (1968).

⁴ C. F. Moore, *Phys. Letters* **25**, 408 (1967).

⁵ E. F. Alexander, C. E. Watson, and N. Shelton, *Nucl. Phys.* (to be published).

⁶ J. L. Weil, M. Cosack, M. T. McEllistrem, J. C. Norman, and M. M. Stautberg, *Bull. Am. Phys. Soc.* **12**, 1196 (1967).

⁷ D. G. Martin and S. A. A. Zaidi, *Bull. Am. Phys. Soc.* **12**, 1196 (1967).

⁸ L. S. Michelman and C. F. Moore, *Phys. Letters* **26**, 446 (1968).

⁹ R. G. Clarkson and W. R. Coker, *Bull. Am. Phys. Soc.* **13**, 631 (1958); and unpublished.

¹⁰ W. R. Coker and C. F. Moore, *Bull. Am. Phys. Soc.* **13**, 631 (1968).

¹¹ Center for Nuclear Studies Annual Report, 1967 (unpublished); R. G. Clarkson, Ph.D. dissertation, University of Texas, 1968 (unpublished); R. G. Clarkson, W. R. Coker, T. A. Griffy, and C. F. Moore, Center for Nuclear Studies Technical Report No. 4, 1968 (unpublished).

¹² S. A. A. Zaidi and P. von Brentano, *Phys. Letters* **23**, 466 (1966).

¹³ T. Tamura and C. E. Watson, *Phys. Letters* **25**, 186 (1967).

¹⁴ A. M. Lane, *Nucl. Phys.* **35**, 676 (1962).

¹⁵ N. Cue and P. Richard, *Phys. Rev.* **173**, 1108 (1968).

¹⁶ E. W. Hamburger, *Phys. Rev. Letters* **19**, 36 (1967).

¹⁷ R. H. Siemssen, G. C. Morrison, B. Zeidman, and H. Fuchs, *Phys. Rev. Letters* **16**, 1050 (1966).

¹⁸ A. Marusak and F. G. Perey (private communication).

¹⁹ H. Fuchs, K. Grabisch, P. Kraaz, and G. Röscher, *Nucl. Phys.* **A110**, 65 (1968).

²⁰ H. Fuchs and R. Santo, *Phys. Letters* **25**, 186 (1967).

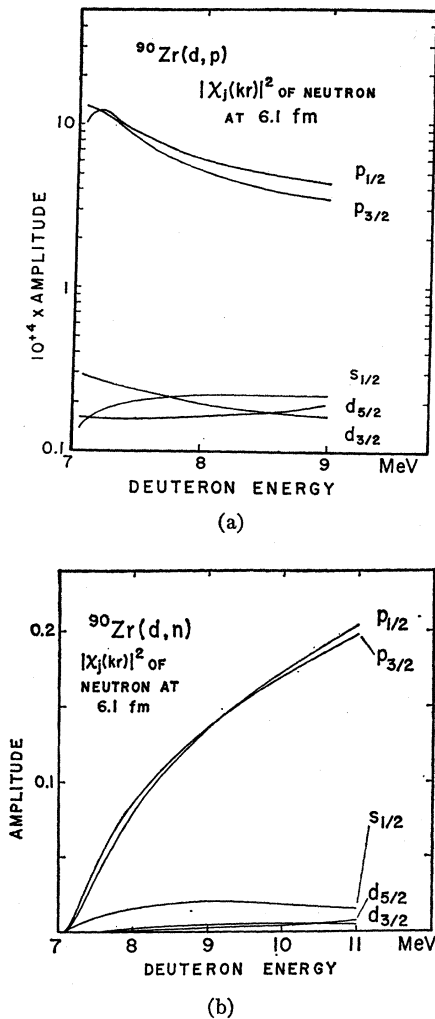


FIG. 1. (a) Amplitudes of s , p , and d neutron partial waves at 6.1 fm, for ${}^{90}\text{Zr}(d, p){}^{91}\text{Zr}$, in the energy region above the ${}^{90}\text{Zr}(d, n){}^{91}\text{Nb}^A$ threshold, according to the Lane equations, with the potentials of Table I. (b) The amplitudes of s , p , and d neutron partial waves at 6.1 fm, for ${}^{90}\text{Zr}(d, n){}^{91}\text{Nb}^A$, according to the Lane equations, with the potentials of Table I. See Sec. II.

wave function of the deuteron, normally eliminated along with the n - p interaction V_{np} by the zero-range approximation $V_{np}\phi_d \sim \epsilon_0\delta(\mathbf{r}_{np})$.

The coupled-channel Born approximation (CCBA) for the same process would be

$$M^{CC} = \langle \hat{\chi}_p^{(-)}\phi_p^\alpha | V_{np} | \chi_d^{(+)}\phi_d \rangle - (2T+1)^{-1/2} \langle \hat{\chi}_n^{(-)}\phi_n^\alpha | V_{np} | \chi_d^{(+)}\phi_d \rangle. \quad (2)$$

Here $\hat{\chi}_p^{(-)}$ and $\hat{\chi}_n^{(-)}$ are the two solutions to the two coupled Lane equations. ϕ_n^α is again the usual shell-model bound state, unless otherwise noted, with binding energy equal to the experimental separation energy. ϕ_p^α is the state function of the isobaric analog of the state represented by ϕ_n^α . The minus sign arises from the assumption that the deuteron is in an isospin state with $I_a=0$. The factor $(2T+1)^{-1/2}$ is required explicitly, to

normalize the analog state in the same way as the parent neutron state. The physical significance of the two amplitudes is clear, since there can now be two indistinguishable contributions to (d, p) : the direct contribution, represented by the first term, and a quasielastic contribution from (d, n) neutrons converted into protons via the off-diagonal part of the Lane potential, given by the second term.

Similarly, for (d, n) reactions,

$$M^{CC} = \langle \hat{\chi}_n^{(-)}\phi_p^\alpha | V_{np} | \chi_d^{(+)}\phi_d \rangle - (2T+1)^{1/2} \langle \hat{\chi}_p^{(-)}\phi_n^\alpha | V_{np} | \chi_d^{(+)}\phi_d \rangle. \quad (3)$$

For purposes of the CCBA calculations reported here, the state function ϕ_p^α was calculated exactly within the Lane model, by solving the bound-state Lane equations,²¹ in the two examples considered in which the analog state is bound: ${}^9\text{Be}(d, n){}^{10}\text{B}$, and ${}^{26}\text{Mg}(d, n){}^{26}\text{Al}$. For the other reactions, ϕ_p^α was approximated as explained in Ref. 13, using a matching radius R_c , which is treated as an adjustable parameter. (A discussion of the use of R_c is given in Sec. VI.)

M^{CC} must be evaluated for a wide range of incident deuteron energies in order to obtain an excitation curve. For E_d less than the (d, n) threshold, $\hat{\chi}_n^{(-)} \rightarrow \phi_n$ is a negative energy state. For E_d greater than the threshold, we have a propagating neutron. Exactly at threshold, we are dealing with a zero-energy neutron, and it might be foreseen that details of the neutron strength function will be of importance in understanding the observed phenomena.

For completeness, we may mention that the CCBA calculation described here is a special case of the general CCBA formulation originally given by Penny and Satchler.²² Incidentally, in solving the Lane equations for Eq. (2), $\hat{\chi}_p^{(+)}$ is matched asymptotically to an outgoing plane wave; for Eq. (3), it is $\hat{\chi}_n^{(+)}$ which is matched. The reader should keep this in mind when comparing Figs. 1(a) and 1(b).

III. THRESHOLD EFFECTS

A. Review of (d, p) Results

The initial suggestion that charge-exchange effects might couple analogous (d, p) and (d, n) channels was given in the original paper of Moore *et al.*,¹ which reported the experimental observation of an abrupt rise in the ${}^{90}\text{Zr}(d, p){}^{91}\text{Zr}(d_{5/2} \text{ ground state})$ excitation curve at 170° , beginning at the ${}^{90}\text{Zr}(d, n)$ threshold to the $d_{5/2}$ analog in ${}^{91}\text{Nb}$. Such experiments¹⁻¹¹ remain among the most impressive evidence for such coupling.

A preliminary CCBA calculation has previously been reported¹³ resulting in a qualitative fit to the $d_{5/2}$ excitation curve of Ref. 1. A large number of CCBA calculations have since been performed, with more

²¹ R. Stock and T. Tamura, Phys. Letters 22, 304 (1966).

²² S. K. Penny and G. R. Satchler, Nucl. Phys. A53, 145 (1964).

complete ^{90}Zr data for comparison than were available previously. Excitation curves, for deuteron energies 5.0–10.5 MeV, at laboratory angles of 80° and 155° for the ^{91}Zr $d_{5/2}$ ground state, $s_{1/2}$ (1.21 MeV), $d_{3/2}$ (2.06 MeV), and $g_{9/2}$ (2.19 MeV) excited states were particularly useful.¹¹ Data at 165° are also available for $^{92,94}\text{Zr}(d, p)$ and $^{92,94}\text{Mo}(d, p)$ to ground $d_{5/2}$ and first $s_{1/2}$ states.³

Several facts about the threshold effect are striking, and worth summarizing. First, the effect becomes progressively weaker as the angle decreases, becoming almost unnoticeable experimentally at 130° in all cases so far considered. Second, the effect (in the $A \approx 80$ –100 region) is strongest in the ground-state excitation curve, and rapidly becomes unnoticeable as one goes to higher and higher excited states. In the 155° and 170° excitation curves for $^{90}\text{Zr}(d, p)^{91}\text{Zr}$, there is a strong anomaly and thus a large departure from DWBA predictions for the $d_{5/2}$ ground state, but the effect is unimpressive in the $s_{1/2}$ (1.21 MeV) state and almost unnoticeable in the $d_{3/2}$ (2.06 MeV) state. Compare Figs. 3 and 6.

Both features of the threshold effect are understandable on the basis of the mechanism originally suggested,^{1,12} as borne out by CCBA calculations. The shape and magnitude of the (d, p) angular distribution are controlled predominantly by the kinematics of specific momentum transfer in the forward angles, but Coulomb and nuclear interactions become extremely important away from the stripping peaks. At back angles, where the stripping contribution becomes very small, the cross section is sensitive to details of the interaction. Indeed, a difficulty in fitting back-angle excitation curves is that the DWBA does not, in general, give a good fit past 130° , particularly if average or extrapolated optical-potential parameters are used.

The second feature is more subtle. It turns out to be important for the incident deuteron near threshold to be well below the nuclear Coulomb barrier. Even when a CCBA calculation is done, the change in the direct (d, p) contribution to the cross section near threshold is small, and the burden of the effect is borne by the charge-exchange (d, n) contribution; usually, only a single neutron partial wave has a significant amplitude and threshold variation with energy.¹³ In the ^{90}Zr region this is the neutron p wave. See Fig. 1. If the overlap integrals involving the p -wave neutron make up an important fraction of the total number of integrals contributing, one expects a noticeable effect; otherwise, not. The former condition holds if the incident deuteron energy E_d is below the Coulomb barrier, since few deuteron partial waves are then important.

As a rule of thumb, which has had considerable predictive value, no threshold effect is seen for a given residual state if the (d, p) Q value for excitation of that state satisfies $Q \leq \frac{1}{4}\Delta_c$, where Δ_c is the Coulomb energy of the residual nucleus. Since the (d, p) threshold is at $E_{d\text{thresh}} = \Delta_c - Q$ and the Coulomb barrier height is

roughly $B_c \approx \frac{3}{4}\Delta_c$, the physical meaning of the rule is obvious.

Finally, we discuss briefly the A dependence of the phenomenon. While only the $^{90}\text{Zr}(d, p)^{91}\text{Zr}$ and $^{92}\text{Mo}(d, p)^{93}\text{Mo}$ cases are discussed here, data are available from $A \approx 80$ –100 and from $A \approx 40$ –50. The p -wave neutron strength function peaks at mass 90. Thus if our understanding of the effect is correct, the magnitude of the departure from the expected shape will diminish as A either decreases or increases from mass 90. This important prediction¹⁴ has now been verified with $^{80}\text{Se}(d, p)^{81}\text{Se}$ ² and $^{96}\text{Zr}(p, d)^{95}\text{Zr}$ ²³ excitation function data for the ground states ($p_{3/2}$ and $d_{5/2}$, respectively), at 160° . In both cases, an effect remains associated with the threshold, though as predicted it is very much weaker than in the ^{90}Zr example. A similar behavior is possibly seen in the region of the s -wave neutron strength function peak at $A \approx 50$, when $^{40}\text{Ar}(d, p)^{41}\text{Ar}$ ⁶ and $^{52}\text{Cr}(d, p)^{53}\text{Cr}$ ¹⁰ data are compared, although the anomalous behavior is much less clear cut in this region because of large-scale fluctuations. When $A > 120$, say, we expect no effect to be observed in any case, since the condition $Q > \frac{1}{4}\Delta_c$ cannot be satisfied even for the ground-state transition.

B. $(d, n\bar{p})$ Cross Section, $A \approx 90$

Proton decay of analog states formed in the (d, n) reaction on a number of targets in the $A \approx 90$ region has been observed by Cue and Richard.¹⁵ Excitation functions were obtained at $\theta_{\text{lab}} = 170^\circ$, from the thresholds up to ~ 17 MeV. Angular distributions were also taken. Of more interest here, however, are data for the total $(d, n\bar{p})$ cross sections, which can be related directly to the total (d, n) cross sections, calculated by CCBA.

One might expect to see some effect due to charge exchange at back angles, in the (d, n) excitation function near threshold, because of coupling with (d, p) . However, (d, n) data are not available, and in any case the charge-exchange effect might not manifest itself as other than an imperceptible variation in the already steeply upward-sloping excitation curve just above threshold. It is nonetheless interesting to see the relative success of DWBA and CCBA calculations in fitting the Cue-Richard total cross-section data.

The total cross section $\sigma(\bar{p})$ for proton decay to a given residual state is related to the total cross section for the formation of the analog state via (d, n) , $\sigma(d, n)$, by $\sigma(\bar{p}) = R(\bar{p})\sigma(d, n)$, where $R(\bar{p})$ is the branching ratio for decay through the particular \bar{p} channel under consideration.¹⁵ It is to be expected that the angle integration required to obtain $\sigma(d, n)$ from the calculated differential cross section will wash out all effects of the charge-exchange process. However, the fitting of the $(d, n\bar{p})$ total cross-section data is still a useful test of the theory, as will be seen.

²³ L. S. Michelman, T. I. Bonner, and J. G. Kulleck, Phys. Letters 28, 659 (1969).

TABLE I. Optical potentials. For all coupled-channel calculations, a Lane potential of the surface type was chosen such that, in the notation of Ref. 32, $V_1=108$ MeV, and $V_1'=V_1R/na$. Thus, $V_1'\approx V_1$.

Channel	V (MeV)	r (fm)	a (fm)	W' (MeV)	r' (fm)	a' (fm)	V_{so} (MeV)	r_{so} (fm)	a_{so} (fm)	r_c (fm)	Ref.
${}^9\text{Be}+d$	118.0	0.886	0.907	5.80	1.57	0.77	5.8	0.907	0.886	1.30	29
${}^{10}\text{B}+n$	45.0	1.32	0.57	11.0	1.32	0.345	5.0	1.32	0.345	1.32	29
${}^{10}\text{Be}+p$											
${}^{25}\text{Mg}+d$	80.0	1.15	0.84	15.0	1.34	0.68	0.0	1.30	19
${}^{26}\text{Al}+n$	44.4	1.305	0.66	4.36	1.258	0.48	0.0	1.305	19
${}^{26}\text{Mg}+p$											
${}^{58}\text{Ni}+d$	111.8	1.05	0.86	17.5	1.32	0.69	6.8	0.75	0.4	1.25	36
${}^{60}\text{Cu}+n$	45.0	1.25	0.65	11.0	1.25	0.47	7.50	1.25	0.65	1.25	18
${}^{60}\text{Ni}+p$											
${}^{90}\text{Zr}+d$	94.5 ^a	1.28	0.72	15.95	1.41	0.694	0.00	1.30	11
${}^{91}\text{Zr}+p$	53.0	1.25	0.65	13.5	1.25	0.47	6.75	1.20	0.42	1.25	11
${}^{91}\text{Nb}+n$	52.0	1.27	0.66	8.10 ^b	1.27	0.47	7.20	1.27	0.66	1.27	
${}^{92}\text{Mo}+d$	88.0	1.28	0.72	14.0	1.41	0.694	0.0	1.3	11
${}^{93}\text{Mo}+p$	54.2	1.22	0.607	5.4	1.293	0.737	7.9	1.12	0.47	1.22	11
${}^{93}\text{Tc}+n$	51.0	1.27	0.66	8.10 ^b	1.27	0.47	7.20	1.27	0.66	1.27	

^a $V(E) = V - \alpha E$ and $\alpha = 1.2$.

^b Below neutron threshold, $W' \rightarrow 0.0$.

C. CCBA Calculations for (d, p) and $(d, n\bar{p})$

CCBA calculations have been performed for the reactions ${}^{92}\text{Mo}(d, p){}^{93}\text{Mo}$ ($d_{5/2}$ ground state)³ and ${}^{92}\text{Mo}(d, n\bar{p})$ ¹⁵ proceeding through the $d_{5/2}$ analog in ${}^{93}\text{Tc}$, using the potentials given in Table I. The deuteron and proton optical potentials are extrapolated from Refs. 24 and 11. The neutron potential is discussed later.

The fits to the available data are shown in Fig. 2. A radius of $R_c = 9.5$ fm was used. It was pleasing that the choice of any other value for this radius gave a very much poorer fit to both (d, p) and $(d, n\bar{p})$ data. Indeed, the calculated shapes are very sensitive to this parameter, and one would have little confidence in them were such agreement not seen. In the ${}^{92}\text{Mo}(d, n\bar{p})$ example, Fig. 2(b), the same theoretical result is obtained with or without coupling, so that with the optical potentials known only R_c may be varied to fit the data. Since the R_c obtained in this way is unique, we believe it is meaningful that the same R_c , used in the (d, p) CCBA, with the same potentials, gives a good description of the (d, p) data at 165° .

Although a vast amount of experimental data is available on the ${}^{90}\text{Zr}(d, p)$ reaction, and numerous DWBA analyses are found in the literature, it proved impossible to find there a single set of optical potentials for deuteron and proton channels giving an adequate description of the available data from 5 to 12 MeV

incident deuteron energy. Therefore, the results of a recent and detailed analysis by Clarkson¹¹ were utilized. Clarkson performed optical-model analyses of deuteron elastic scattering from ${}^{90,91,92}\text{Zr}$ at 5–12 MeV, and proton elastic scattering from the same targets at 10–13 MeV.

A neutron potential was obtained by fitting the p -wave neutron strength function in the mass-90 region; the resulting potential is similar to one suggested by Buck and Perey.²⁵ No single potential could be found which described both proton elastic scattering and the neutron strength function, whether a symmetry term was included or not. The potentials are summarized in Table I.

The ${}^{90}\text{Zr}$ data are surprisingly difficult to describe with the present theory. The moderate success of the calculation presented in Ref. 13 is not preserved when minor numerical errors committed therein are corrected. However, just as in the ${}^{92}\text{Mo}$ case, a particular choice of R_c is found to provide a reasonable good description both (d, p) and $(d, n\bar{p})$ data. Figure 3(a) shows 155° data for ${}^{90}\text{Zr}(d, p){}^{91}\text{Zr}$ ($d_{5/2}$ ground state), and DWBA and CCBA predictions using the potentials of Table I. Figure 3(b) illustrates the CCBA fit for ${}^{90}\text{Zr}(d, n\bar{p})$ data of Ref. 15. Finally, in Fig. 4 are shown the fits to the ${}^{90}\text{Zr}(d, p)$ $d_{5/2}$ ground-state excitation curve at 170 and 110° .

²⁴ J. K. Dickens and E. Eichler, Nucl. Phys. **A101**, 408 (1967).

²⁵ B. Buck and F. G. Perey, Phys. Rev. Letters **8**, 444 (1

In order to produce the agreement with experiment shown in Figs. 3 and 4 in the region 6–7 MeV, it was necessary to vary the surface imaginary depth of the neutron optical potential with energy smoothly from 0.0 MeV, at 6.25 MeV, to its threshold value of 8.1 MeV. The only other part of any optical potential which was varied with energy in these calculations was the real-well depth of the deuteron optical potential. In the work of Clarkson, and herein, an energy dependence of the form $V = V_0 - \alpha E$ was used in fitting the (d, d) elastic data from 5 to 12 MeV.¹¹

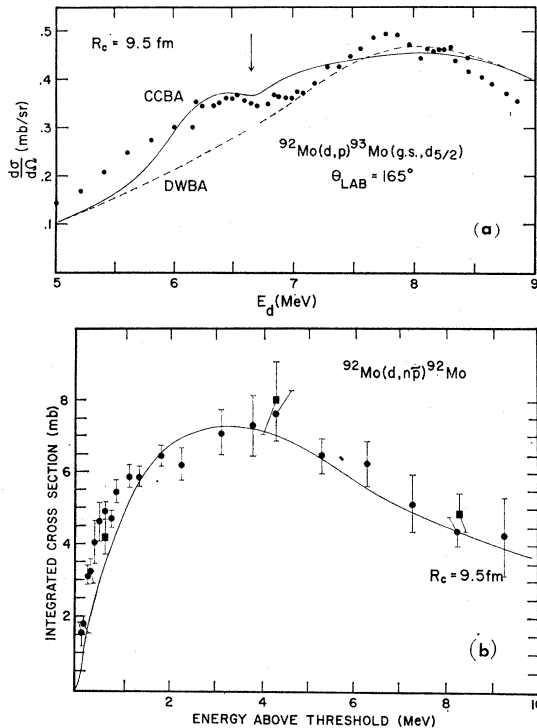


FIG. 2. (a) $^{92}\text{Mo}(d, p)^{93}\text{Mo}(d_{5/2}$ ground state) excitation function at 165° , from Ref. 3. The solid line is a CCBA calculation with $R_c = 9.5$ fm and the potentials given in Table I. The dashed line is an ordinary DWBA calculation using the same potentials. Normalization is absolute. (b) $^{92}\text{Mo}(d, np)^{92}\text{Mo}$ integrated cross section, from Ref. 15. The solid line is the integrated $^{92}\text{Mo}(d, n)^{92}\text{Tc}^A$ cross section calculated by CCBA with $R_c = 9.5$ fm and the potentials of Table I, arbitrarily normalized.

Clarkson *et al.*¹¹ obtained $^{90}\text{Zr}(d, p)$ excitation curves at $80^\circ, 95^\circ, 110^\circ, 140^\circ, 155^\circ$, and 170° , from 5.0 to 10.9 MeV incident deuteron energy, for nine states in ^{91}Zr . In Fig. 5 are shown the 155° excitation curves for 1.21-MeV $s_{1/2}$ and 2.06-MeV $d_{3/2}$ states, illustrating the Q -value rule stated in Sec. III A. We have $\frac{1}{4}\Delta_c = 3.0$ MeV, while $Q(s_{1/2}) = 3.76$ MeV and $Q(d_{3/2}) = 2.9$ MeV. As expected, no threshold effect is noticeable in the $d_{3/2}$ excitation-function data. Since no (d, np) data are available, the CCBA results in Fig. 5 are shown for various choices of R_c . A radius somewhat less than 6.5 fm is seen to be satisfactory in both cases. The

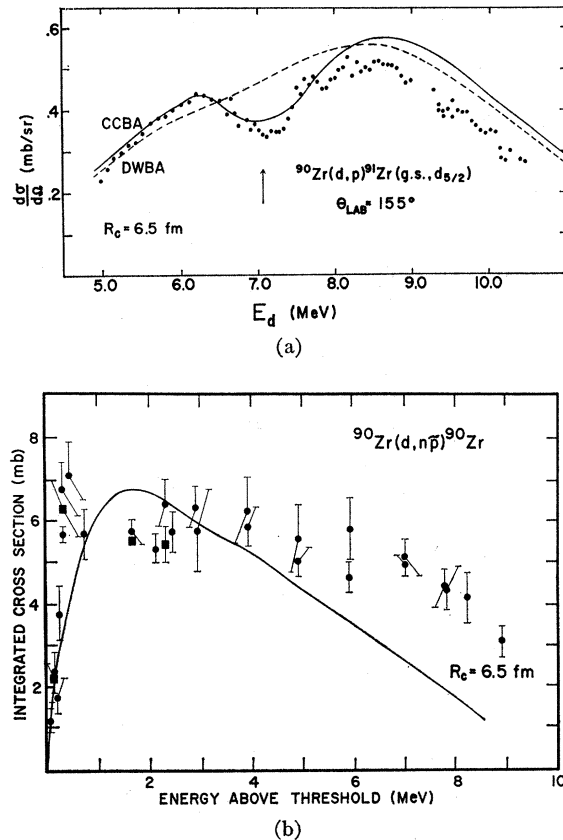


FIG. 3. (a) $^{90}\text{Zr}(d, p)^{91}\text{Zr}(d_{5/2}$ ground state) excitation function at 155° , from Ref. 11. The solid line is a CCBA calculation with $R_c = 6.5$ fm and the potentials given in Table I. The dashed line is an ordinary DWBA calculation using the same potentials. Normalization is absolute. (b) $^{90}\text{Zr}(d, np)^{90}\text{Zr}$ integrated cross section, from Ref. 15. The solid line is the integrated $^{90}\text{Zr}(d, n)^{91}\text{Nb}^A$ cross section calculated by CCBA with $R_c = 6.5$ fm and the potentials of Table I, arbitrarily normalized.

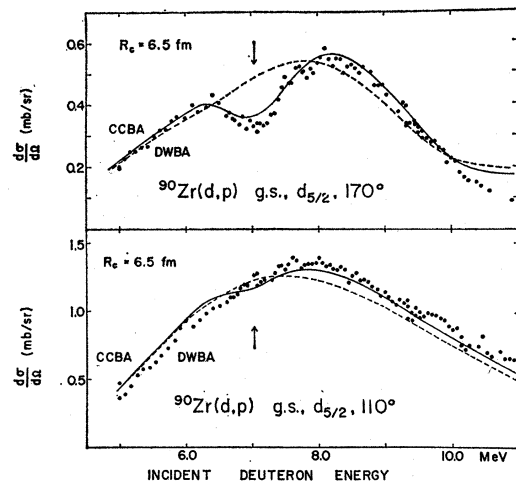


FIG. 4. $^{90}\text{Zr}(d, p)^{91}\text{Zr}(d_{5/2}$ ground state) excitation function at 110° and 170° , illustrating the angle dependence of the threshold effect as discussed in Sec. III A. The solid line is the CCBA calculation with $R_c = 6.5$ fm, and the dashed line a corresponding DWBA calculation, in both cases. Potentials are those of Table I.

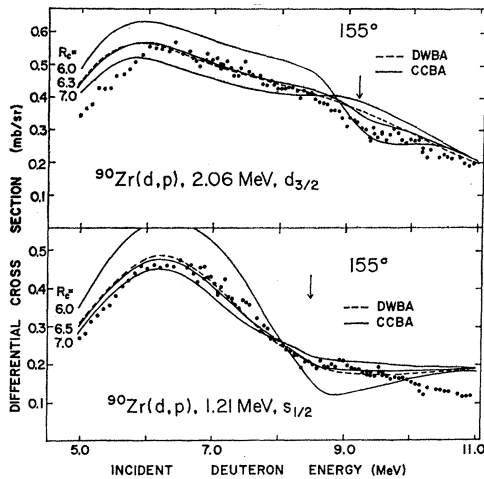


FIG. 5. $^{90}\text{Zr}(d, p)^{91}\text{Zr}$ (1.21 MeV $s_{1/2}$ and 2.06 MeV $d_{3/2}$) excitation functions at 155° , illustrating the Q dependence of the threshold effect as discussed in Sec. III A. The solid lines are CCBA calculations for various choices of R_c . The dashed line is the usual DWBA result. The potentials are those of Table I. Normalization is absolute.

vertical arrow appearing in Figs. 3–5 marks the position of the appropriate (d, n) threshold.

In Fig. 6 is shown the result of using the proton potential of Ref. 13 in both nucleon channels. Such a potential predicts the p -wave neutron strength function peak at about mass 110. Note that an effect remains associated with the (d, n) threshold, and that a second minimum occurs near 9.5 MeV.

For all coupled-channel calculations discussed in this and the next two sections, a surface-type Lane potential was chosen, with a depth in each case such that in the proton channel it has a strength of $27(N-Z)/A$ MeV. See Table I.

IV. EFFECT OF ANALOG RESONANCES IN (d, p)

Hamburger¹⁶ observed a marked energy dependence in $^{207}\text{Pd}(d, p)^{208}\text{Pb}$ excitation curves, at deuteron energies such that an isobaric analog resonance is excited in the outgoing proton channel. We shall show briefly that this phenomenon can be fairly well described within the framework of the CCBA as developed in Sec. II. The analysis given here has been summarily reported previously,²⁶ and is included for completeness.

It may seem obvious that if a strong resonance occurs in the proton channel, its effect will be observed readily in the (d, p) excitation curve. However, the isobaric analog resonance is a very special type of resonance, and Hamburger's observation of the anomaly in (d, p) is in fact quite surprising when conservation of isobaric spin is considered. In the incident channel, the total isospin is just the isospin T_t of the target, since $t_d=0$. In the $^{207}\text{Pb}(d, p)^{208}\text{Pb}$ case, $T_t=43/2$. However, the analog

resonance in the $^{208}\text{Pb}+p$ system has $T=45/2$, and we should not expect a resonance in (d, p) .

We want to show that the expression for M^{CC} [Eq. (2)] allows such an anomaly. First note that M^{CC} can be written as $M_{>}^{\text{CC}}+M_{<}^{\text{CC}}$, where $M_{>}^{\text{CC}}$ is obtained from Eq. (2) by replacing $\hat{\chi}_p^{(-)}$ and $\hat{\chi}_n^{(-)}$ by $\hat{\chi}_{p,>}^{(-)}$ and $\hat{\chi}_{n,>}^{(-)}$, respectively. $M_{<}^{\text{CC}}$ is similarly defined. $\hat{\chi}_{p,>}^{(-)}$ and $\hat{\chi}_{n,>}^{(-)}$ are the solutions of the Lane equations with $T=T_t+1$, $\hat{\chi}_{p,<}^{(-)}$ and $\hat{\chi}_{n,<}^{(-)}$ the solutions with $T=T_t$. Thus we get

$$M_{>}^{\text{CC}} = \langle \hat{\chi}_{p,>}^{(-)} \phi_n^\alpha | V_{np} | \chi_d^{(+)} \phi_d \rangle - (2T+1)^{-1/2} \langle \hat{\chi}_{n,>}^{(-)} \phi_p^\alpha | V_{np} | \chi_d^{(+)} \phi_d \rangle, \quad (4)$$

and the analogous equation for $M_{<}^{\text{CC}}$.

The familiar expression symbolized as (analog state) = T_- (parent state) requires that

$$\phi_n^\alpha = \phi_p^\alpha \quad \text{and} \quad \hat{\chi}_{p,>}^{(-)} = (2T+1)^{-1/2} \chi_{n,>}^{(-)}, \quad (5)$$

so that $M_{>}^{\text{CC}}=0$. The isospin selection rule is thus already built into Eq. (2).

However, the Lane equations do not conserve isospin. This means, in particular, that the second equality in (5) does not hold over all space. Indeed, its violation becomes significant in the region just outside the nuclear surface, which is the region where the largest contributions to the (d, p) stripping process arise. It is to be expected, then, that the CCBA as embodied in Eq. (2) will explain the phenomenon observed by Hamburger.

In Fig. 7(a) the CCBA excitation curves are compared with Hamburger's data, while in Fig. 7(b) the $^{208}\text{Pb}(p, p)$ data of Zaidi *et al.*²⁷ are compared with the

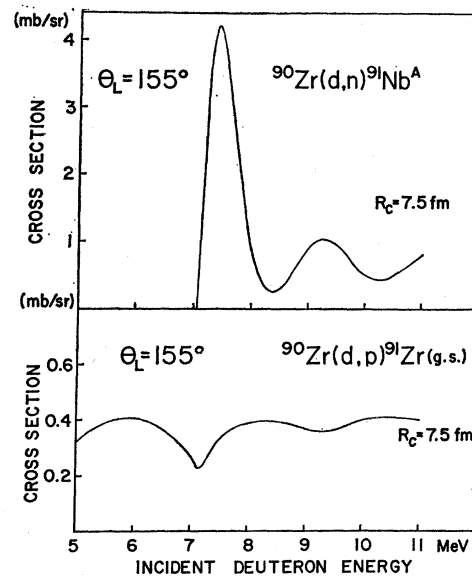


FIG. 6. $^{90}\text{Zr}(d, p)^{91}\text{Zr}$ ($d_{5/2}$ ground state) and $^{90}\text{Zr}(d, n)^{91}\text{Nb}^A$ ($d_{5/2}$ analog) cross sections at 155° , using the potential of Ref. 13 in both nucleon channels.

²⁷ S. A. A. Zaidi, J. L. Parish, J. G. Kulleck, C. F. Moore, and P. von Brentano, Phys. Rev. **165**, 1312 (1968).

²⁶ T. Tamura, J. Phys. Soc. Japan Suppl. **24**, 288 (1967).

predicted elastic scattering in the proton channel, calculated by straightforward solution of the Lane equations.²⁸ The functions $\chi_p^{(-)}$ and $\chi_n^{(-)}$, obtained by fitting the region of the analog resonance in this way, were used in Eq. (2) to obtain the CCBA results shown in Fig. 7(a). The agreement is by no means perfect, but shows that our approach is basically correct. A significant aspect of the calculation is its demonstration that Hamburger's data may be described completely within the framework of direct reactions, so that it is not necessary to introduce phenomenological resonance terms as originally suggested by Hamburger.¹⁶

V. SPECTROSCOPIC FACTORS

Some time ago, Siemssen *et al.*¹⁷ directed attention to evidence for a systematic discrepancy between the spectroscopic factors extracted from conventional DWBA analysis of (³He, *d*) and (*d*, *n*) reactions on the same target nucleus when the residual nuclear state is an isobaric analog state. Although good agreement is usually found between the spectroscopic factors obtained for, say, the ground state, one may find the ratio of the spectroscopic factors to be $S(d, n)/S(^3\text{He}, d) \approx 0.5$ for the first analog state. It seems natural to investigate what effect a CCBA calculation of the (*d*, *n*) cross section has on this discrepancy.^{29,30} We investigate three cases for which detailed DWBA analyses have previously been carried out.

A. ⁹Be(*d*, *n*)¹⁰B Reaction

For the two reactions ⁹Be(*d*, *n*)¹⁰Be (1.74 MeV, *p*_{3/2}) and ⁹Be(³He, *d*)¹⁰B (1.74 MeV *p*_{3/2}), to the mirror of the ¹⁰Be ground state, one finds $S(d, n) \approx 1.0$, while $S(^3\text{He}, d) \approx 2.5$ in somewhat better agreement with the prediction of Cohen and Kurath,³¹ 2.36. A calculation has been reported by one of us²⁹ which indeed seemed to explain the discrepancy by reducing the CCBA (*d*, *n*) cross section by a factor of 0.44. However, a numerical error was made in the calculation, and the actual state of affairs is rather different. Taking the optical potentials of Ref. 29, and the isospin coupling strength suggested by Satchler *et al.*,³² the result is that the CCBA cross section is *increased* by a factor of 1.35. Thus the discrepancy becomes somewhat worse.

In an effort to understand the result, we changed the sign of the *t*·*T* term, which reduced the CCBA cross section by only 6% relative to DWBA. Even with the coupling term four times the value normally quoted, and of opposite sign, the CCBA/DWBA ratio is only 0.79. Changing the optical potentials, in particular the

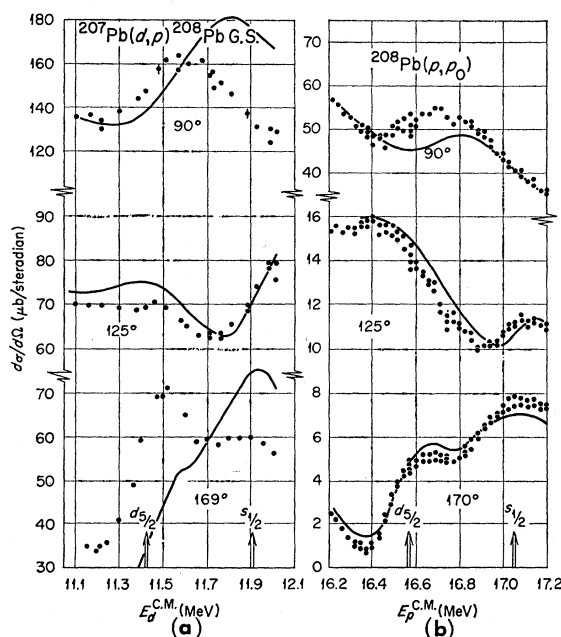


FIG. 7. (a) ²⁰⁷Pb(*d*, *p*)²⁰⁸Pb cross section at 90°, 125°, and 169°. The solid lines are CCBA predictions. (b) Isobaric analog resonances in ²⁰⁸Pb(*p*, *p*) at 90°, 125°, and 170°. The solid lines are obtained by solution of the Lane equations.

neutron surface absorptive potential, which might be expected to be smaller for CCBA, had no meaningful effect. Nor was the shape fit to the (*d*, *n*) angular distribution improved for any of the variations performed.

We conclude that the charge-exchange coupling of analogous (*d*, *p*) and (*d*, *n*) channels does not explain the discrepancy observed in ⁹Be(*d*, *n*)¹⁰B.

B. ²⁵Mg(*d*, *n*)²⁶Al Reaction

As another application of the CCBA we consider the ²⁵Mg(*d*, *n*)²⁶Al¹⁹ and ²⁵Mg(³He, *d*)²⁶Al³³ reactions. The states of interest are the 0⁺ (0.23 MeV) and the 2⁺ (3.16 MeV) levels of ²⁶Al, both of which have *T*=1. ²⁵Mg(*d*, *p*)²⁶Mg data for the parent analogs are also available for comparison.

DWBA analysis is somewhat complicated in this case, since ²⁵Mg is deformed. Nilsson wave functions have been used in the reported analyses^{19,23} but the spectroscopic factors extracted by this means do not show better agreement with theoretical expectations than those given by ordinary spherical shell-model states, which we have therefore used for simplicity in the CCBA calculations.

Table II summarizes the results.³⁴ It is seen that, as in the ⁹Be(*d*, *n*)¹⁰B case; the CCBA result is not appreciably different from the DWBA result, and again yields a

²⁸ T. Tamura, in *Isobaric Spin in Nuclear Physics*, edited by J. Fox and D. Robson, (Academic Press Inc., New York, 1966), p. 447; J. P. Bondorf, H. Lutken, and S. Jägare, *ibid.*, p. 576.

²⁹ T. Tamura, *Phys. Rev. Letters* **19**, 321 (1967).

³⁰ T. Tamura, *Phys. Rev.* **165**, 1123 (1968).

³¹ S. Cohen and D. Kurath, *Nucl. Phys.* **A101**, 1 (1967).

³² G. R. Satchler, R. M. Drisko, and R. H. Bassel, *Phys. Rev.* **136**, B637 (1964).

³³ A. Weidinger, R. H. Siemssen, G. C. Morrison, and B. Zeidman, *Nucl. Phys.* **A108**, 547 (1968).

³⁴ S. Hinds, H. Marchant, and R. Middleton, *Nucl. Phys.* **A67**, 257 (1965); H. F. Lutz and S. F. Eccles, *ibid.* **A88**, 513 (1966).

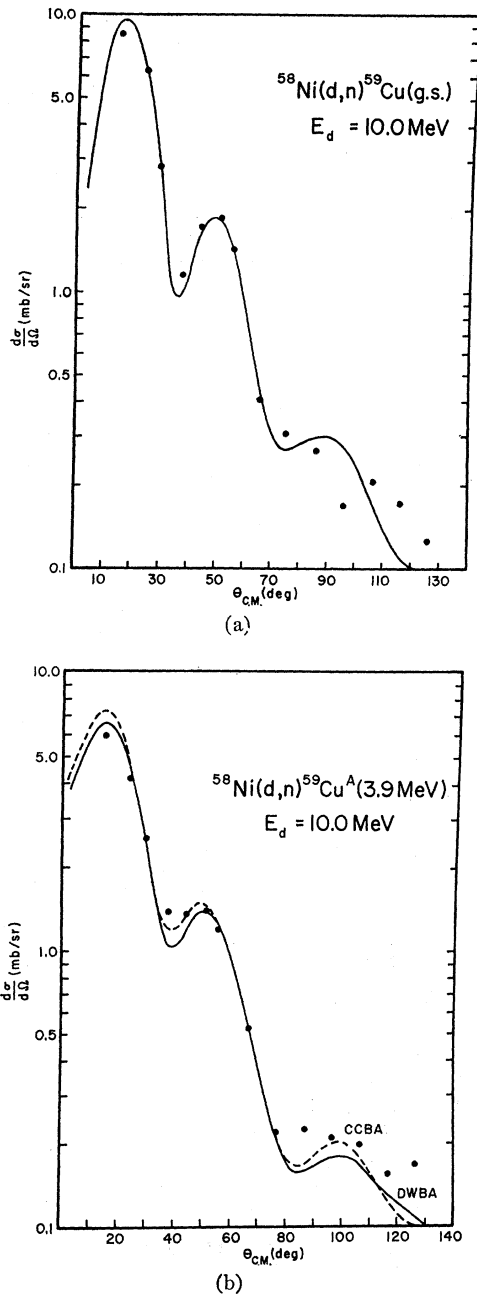


FIG. 8. (a) $^{58}\text{Ni}(d, n)^{59}\text{Cu}$ ($p_{3/2}$ ground state) cross section at $E_d = 10.0$ MeV, from Ref. 18. The DWBA prediction is shown as a solid line. (b) $^{58}\text{Ni}(d, n)^{59}\text{Cu}$ ($p_{3/2}$ analog) cross section at $E_d = 10.0$ MeV, from Ref. 18. DWBA and CCBA calculations, assuming the analog state is bound by 0.5 MeV, are shown as solid and dashed lines, respectively.

spectroscopic factor somewhat smaller, rather than larger. The optical potentials used were those of Ref. 19. See Table I.

C. $^{58}\text{Ni}(d, n)^{59}\text{Cu}$ Reaction

As a final example, we consider the (d, n) reaction on ^{58}Ni , for which angular distributions have recently been

obtained by Perey and Marusak, at $E_d = 5$ and 10 MeV. A great deal of work has been done with $^{58}\text{Ni}(^3\text{He}, d)^{59}\text{Cu}$, and spectroscopic factors are readily available in the literature³⁵ for bound and continuum states up to 7.0-MeV excitation in ^{59}Cu . We consider the $p_{3/2}$ ground state and the just-unbound (by 0.48 MeV) $p_{3/2}$ state at 3.9-MeV excitation, which is presumably the isobaric analog of the ^{58}Ni ground state. Since the Perey-Marusak data had not been previously analyzed, both regular DWBA and CCBA calculations were performed. Excellent fits to the 10.0-MeV angular distributions were obtained using the $^{60}\text{Ni}+d$ potential of Schwandt and Haberli,³⁶ and a neutron potential due to Perey.¹⁸ See Fig. 8. The analog state spectroscopic factor was obtained by smooth extrapolation to the continuum energy, since this was the method used in the $(^3\text{He}, d)$ analyses. The shape fit in Fig. 8 for the analog-state transition was obtained by performing a calculation with very weak binding, 0.5 MeV. Both CCBA and DWBA were normalized by the same factor ($S = 0.332$), so that the difference in magnitude of the two angular distributions is apparent.

The ratio of the analog state spectroscopic factor $S_>$ to that of the ^{59}Cu ground state S_0 is $S_>/S_0 = 0.19$ from two $(^3\text{He}, d)$ analyses,³⁷ in reasonable agreement with the theoretical expectation of 0.17. The result of the (d, n) DWBA analysis is $(S_>/S_0)_{\text{DWBA}} \approx 0.33$. A coupled-channel calculation, assuming normal coupling, gives essentially no change: $(S_>/S_0)_{\text{CCBA}} \approx 0.30$. Thus the discrepancy is not explained. However it is worth noting that the result of a third $(^3\text{He}, d)$ analysis³⁸ gives $(S_>/S_0)_{\text{DWBA}} \approx 0.29$, so that the reality of a discrepancy is unclear in this case.

D. Summary

The three cases considered here are sufficient to lead to the conclusion that although the charge-exchange coupling might be suspected to have a noticeable effect on the magnitude of the (d, n) cross section to an analog state, the direct (d, n) term in fact remains predominant and is essentially unchanged by the coupling, at least in the lighter nuclei ($A < 50$).

VI. GENERAL CONCLUSIONS

In Secs. III and IV, it has been seen that the scheme of Sec. II explains fairly well the anomalous energy dependence of (d, p) cross sections in cases where charge-exchange effects can play a significant role. Section V showed, on the other hand, that CCBA is not sufficient to explain the anomalous $S_>$ spectroscopic factors, particularly for (d, n) reactions. Siemssen³⁹ has stressed that the experimental data bearing upon the $S_>$ anomaly are few as yet, and that drawing conclusions

³⁵ J. Vervier, Nucl. Data Sect. B 2, 34 (1968).

³⁶ P. Schwandt and W. Haberli, Nucl. Phys. A110, 585 (1968).

³⁷ G. Morrison and J. P. Schiffer, in Ref. 28, p. 748; A. G. Blair and D. D. Armstrong, Phys. Letters 16, 57 (1965).

³⁸ D. J. Pullen and B. Rosner, Phys. Rev. 170, 1034 (1968).

³⁹ R. H. Siemssen (private communication).

TABLE II. Absolute spectroscopic factors.

Excitation, J^π (MeV)		Spectroscopic factors			
^{26}Al	^{26}Mg	$(d, p)^a$	$(^3\text{He}, d)^b$	$(d, n)^c$	CCBA(d, n)
0.23, 0^+	0.0, 0^+	1.85	2.46	1.26	1.00
3.16, 2^+	2.96, 2^+	0.14	0.34	0.37	0.30 $l_n=0$
		0.25 \pm 0.14	0.65	0.34 \pm 0.17	... $l_n=2$

^a Reference 34.^b Reference 33.^c Reference 19.

is somewhat dangerous. Nonetheless, it seems unlikely that the sole explanation of the phenomenon rests upon charge exchange. Another explanation must be sought.

An unsatisfactory aspect of the analysis of threshold effects discussed in Sec. III is the use of the adjustable parameter R_c . This arbitrariness was difficult to avoid, for several reasons. Consider for explicitness the $^{90}\text{Zr}(d, p)^{91}\text{Zr}$ example. In order to set up Lane equations for the 92nd nucleon to be solved for $\hat{\chi}_p^{(-)}$ and $\hat{\chi}_n^{(-)}$, we assumed $^{91}\text{Nb}^4 = [T_-(^{91}\text{Zr})]/(2T+1)^{1/2}$. Hence it is required that at least the major portion of ϕ_p^α must be equal to ϕ_n^α [see Eq. (2)]. It is important to notice that ϕ_n^α is a real function, except for an over-all phase. A way to avoid use of R_c is to solve the Lane equations again for the 91st nucleon⁴⁰ but since the proton described by ϕ_p^α is in the continuum, ϕ_p^α is complex. A naive application of the Lane equations is thus dangerous, and we thought it preferable to set $\phi_p^\alpha = \phi_n^\alpha$ exactly for $r \leq R_c$ and to connect ϕ_p^α smoothly with a positive energy Coulomb function for $r > R_c$.

All such problems can be avoided once one has a scheme to construct the wave function of a proton in an isobaric analog resonance, since this is precisely the residual state ϕ_p^α . An approach which seems plausible is the introduction of the so-called "ideal analog state" ψ_p^α which is obtained by literally operating with T_- upon the parent neutron state. The equality $\psi_p^\alpha = \phi_n^\alpha$ is then exact over all space. In the language of the shell-model approach to nuclear reactions,⁴¹ ψ_p^α is a bound state embedded in the continuum, to which it is coupled. Introducing the continuum wave functions $\psi_p^{(+)}(E)$, the "real analog state" ϕ_p^α is given as

$$\phi_p^\alpha = \psi_p^\alpha + \int_0^\infty a(E) \psi_p^{(+)}(E) dE, \quad (6)$$

where the mixing coefficient $a(E)$ can be calculated exactly, in principle, given a shell-model Hamiltonian. ϕ_p^α , as defined by Eq. (6), has the requisite properties to describe the resonant state.

⁴⁰ J. Zimanyi and B. Gyarmati, Phys. Letters 27, 120 (1968).⁴¹ U. Fano, Phys. Rev. 124, 1866 (1961).

Recall that in fitting $^{90}\text{Zr}(d, p)$ and $^{92}\text{Mo}(d, p)$ data simultaneously, quite different values of R_c had to be used: $R_c \approx 9.5$ fm for ^{92}Mo and $R_c \approx 6.5$ fm for ^{90}Zr . The radically differing $(d, n\bar{p})$ total cross sections for these two nuclei suggest that we take this difference in R_c seriously. The explanation of the observed differences thus lies in ϕ_p^α . In the language of Eq. (6), a decreasing R_c represents an increasing contribution from the second term, representing coupling to the continuum. Thus the $^{91}\text{Nb}^4$ state is required to be coupled more strongly to the continuum than the $^{93}\text{Tc}^4$ state. This result is consistent with the energetics of the two systems.

The Coulomb displacement Δ_c for the $^{91}\text{Zr}-^{91}\text{Nb}^4$ system is about 11.9 MeV. For the $^{93}\text{Mo}-^{93}\text{Tc}^4$ system it is 12.4 MeV, so that the Coulomb barrier is half an MeV higher in the latter case. However, the ground-state analog \bar{p} decay c.m. energy is 4.7 MeV for $^{91}\text{Nb}^4$, and 4.3 MeV for $^{93}\text{Tc}^4$.⁴² Thus the decaying $^{93}\text{Tc}^4$ proton is effectively handicapped by an MeV, relative to the $^{91}\text{Nb}^4$ proton, in penetrating the Coulomb barrier. It is quite plausible that the $^{93}\text{Tc}^4$ state has a considerably longer lifetime, as compared to $^{91}\text{Nb}^4$, i.e., that the second term of Eq. (6) is small. It is to be expected, then, that $R_c(^{93}\text{Tc}^4) > R_c(^{91}\text{Nb}^4)$.

The development of a theory of isobaric analog resonances based on the shell-model approach⁴³ is now under way by one of us (T.T.). It is intended that ϕ_p^α can be evaluated as indicated by Eq. (6). It will then be possible to redo and extend the calculations reported in Sec. III, using the improved ϕ_p^α . Also, the availability of such a resonance theory will permit reanalysis of such (d, p) data as Hamburger's, discussed in Sec. IV, by improving the description of the state of the 209th nucleon. It is hoped that the role of the isospin selection rule can be made transparent in such a description of the process.

⁴² D. D. Long, P. Richard, C. F. Moore, and J. D. Fox, Phys. Rev. 149, 906 (1966).⁴³ T. Tamura, in *Proceedings of the International Symposium on Nuclear Structure, Dubna* (International Atomic Energy Agency, Vienna, 1968), p. 213; Phys. Rev. (to be published).